
A Successive LP Approach with C-VaR Type Constraints for IMRT Optimization

Shogo Kishimoto¹ and Makoto Yamashita²

Submitted: December 5, 2016.

Abstract: Radiation therapy is considered to be one of important treatment protocols for cancers. Radiation therapy employs several beams of ionizing radiation to kill cancer tumors, but such irradiation also causes damage to normal tissues. Therefore, a treatment plan should satisfy dose-volume constraints (DVCs). Intensity-modulated radiotherapy treatment (IMRT) enables to control the beam intensities and gives more flexibility for the treatment plan to satisfy the DVCs. Romeijn et al. [Physics in Medicine and Biology, 48(21):3521, 2003] replaced the DVCs in an IMRT optimization with C-VaR (Conditional Value-at-Risk) type constraints, and proposed a numerical method based on linear programming (LP). Their approach reduced the computation cost of the original DVCs, but the feasible region of their LP problems was much narrow compared to the DVCs, therefore, their approach often failed to find a feasible plan even when the DVCs were not so tight.

In this paper, we propose a successive LP approach with the C-VaR type constraints. We detect outliers from the solution of LP problems, and remove them from the domain of the C-VaR type constraints. This eases the sensitivity of C-VaR type constraints to outliers and we can search feasible plans from wider regions. Furthermore, we can give a mathematical proof that if the optimal value of the LP problem in the proposed approach is non-positive, the corresponding optimal solution satisfies all the DVCs. From numerical experiments on test data sets, we observed that our approach found feasible solutions more appropriately than existing LP approaches. In addition, our approach required fewer LP problems, and this led to a short computation time.

Keywords: Intensity-modulated radiotherapy treatment, Fluence map optimization, Linear programming, C-VaR

1 Introduction

In many countries, cancer is considered to be one of the principal causes of death. In Japan, it was reported in [15] that the fatalities number rose to 350 thousand people and 800 thousand people were newly diagnosed as cancer in the year 2010. Prevalent types of cancer treatment include chemotherapy, surgery, and radiation therapy. An investigation conducted by Ministry of Health, Labor and Welfare of Japan [17] reported that their percentages are 81%, 72%, and 32%, respectively (the numbers include combinations of treatment types). National Cancer Institute also reported that half of the cancer patients receive radiation therapy during their treatment [14]. Radiation therapy is a treatment that uses several beams of ionizing radiation against cancer tumors, using a property that the beam irradiation has effect of reducing or killing cancer tumors.

¹ Department of Mathematical and Computing Sciences, Tokyo Institute of Technology, 2-12-1-W8-29 Ookayama, Meguro-ku, Tokyo 152-8552, Japan (kishimoto.s.ac@m.titech.ac.jp).

² Department of Mathematical and Computing Science, Tokyo Institute of Technology, 2-12-1-W8-29 Ookayama, Meguro-ku, Tokyo 152-8552, Japan (Makoto.Yamashita@is.titech.ac.jp). His research was partially supported by JSPS KAKENHI (Grant Number: 15K00032).

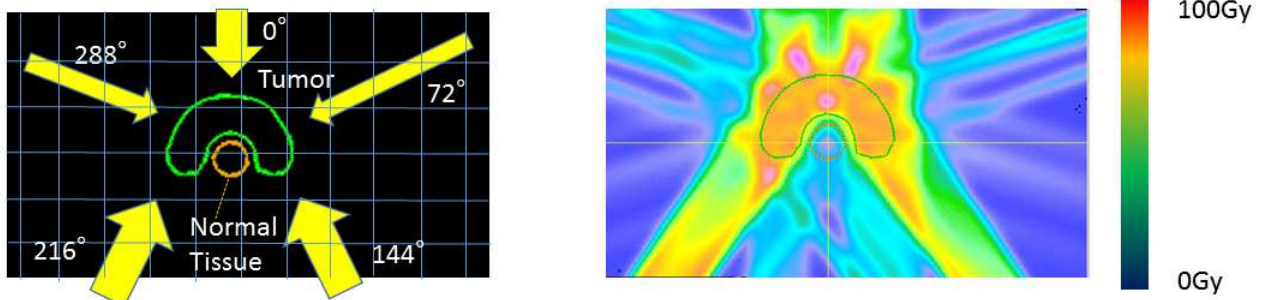


Figure 1: An image of beam intensities for a tumor and normal tissues.

One of the merits of radiation therapy is that patients receive weak damage to the body compared to surgery, and this can bring high possibilities for continuing a normal daily life.

Intensity-modulated radiotherapy treatment (IMRT) has brought a remarkable flexibility in dose irradiated from the beams. With the aid of computers and the usage of devices like multi-collimator, IMRT can control the beam irradiation with higher accuracy than before, and this leads to the high accuracy of the radiation delivery. The irradiation device can continuously rotate around a patient who is on a couch and it irradiates the ionizing radiation at certain angles. In the left figure of Figure 1, the beam is irradiated at the five angles, 0° , 72° , 144° , 216° and 288° . The right figure of Figure 1 shows that, due to an appropriate adjustment of the beam intensities, the tumor receives a high dose and at the same time the normal tissues are kept away from the high dose. The patient, however, can not move during the treatment to increase the irradiation accuracy. In practice, the number of angles during one treatment is limited to four to nine in order to lessen a burden on the patient [9].

The computation of IMRT planning involves several optimization aspects, for example, beam angle optimization (BAO) [3, 7, 10, 28, 12], fluence map optimization (FMO) [2, 24, 26], and direct aperture optimization (DAO) [25, 27]. BAO chooses the best angles from candidate angles on constraints like the number of angles available for one treatment, and FMO is an optimization problem to determine the irradiation intensity for given beam angles. DAO considers the locations of multi-collimator and beam intensity simultaneously. Chapters 4 and 5 of the handbook [21] discussed many aspects on IMRT from the viewpoints of optimization.

A difficulty arising in FMO problems, however, is that not only malignant tumors but also normal tissues near the tumors receive negative effects from the beam irradiation. The oncologists develop treatment plans for the irradiation areas and the beam intensity to reduce the damage onto the normal tissues.

A key criterion of the treatment plans is to satisfy dose-volume constraints (DVCs). A DVC is a radiation-dose constraint on a partial volume of an organ. For example, more than 90% area of the tumor should receives at least 50 Gy (Gy is the international unit of ionizing radiation dose per unit mass; $1 \text{ Gy} = 1 \text{ Joule/kg}$), while the fraction of the normal tissues that receive 25 Gy or higher should be under 10%. Figure 2 shows an example of dose-volume histograms (DVHs) for a cancer tumor and normal tissues near the tumor. The blue line is a histograms for a tumor PTV and the other lines are for Cord, Lt Parotid and Rt Parotid. In Figure 2, the horizontal axis is a dose volume and the vertical axis is the fraction of the structure. The PTV histogram passes the point (50 Gy, 90%), and this indicates that the tumor area that receives 50 Gy or more is 90%. This histogram satisfies a DVC on the tumor which requires that the area that incurs at least 50 Gy takes at least 90% of the tumor (This DVC will be expressed as $L_{\text{PTV}}^{0.90} = 50$ in the notation

that will be introduced in Section 2.1).

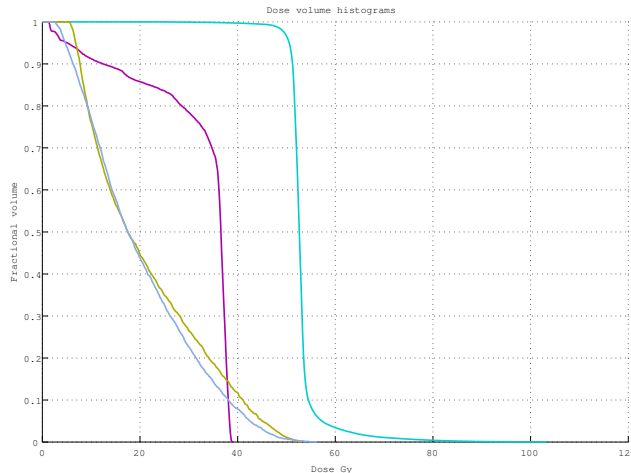


Figure 2: An example of dose-volume histograms for a tumor (PTV) and normal tissues (Cord, Lt Parotid and Rt Parotid).

In general, multiple DVCs can be imposed for one treatment. To find a good treatment plan that satisfies all the DVCs on tumors and normal tissues, a number of approaches based on mathematical optimization methods have been proposed. Morrill et al. [18] employed Linear programming (LP) problems for FMO problems with DVCs. Merrit et al. [16] proposed a successive LP approach. In determining the beam intensity, a few parts of body receive much large dose, and such outliers make it very hard to find a feasible solution. Merrit et al. detected these outliers based on the information of a dual LP problem, and relaxed the dose threshold for the outliers to higher values. Zhang et al. [30] proposed a two-stage sequential LP approach. Aleman et al. [1] solved an optimization problem that minimizes a quadratic objective function which evaluated the deviations from DVCs. They proposed a specific interior-point method to solve this quadratic optimization problem. Hamacher and Küder [13] examined a multiple objective optimization approach. Chu et al. [5] and Olafsson and Wright [20] discussed approaches based on robust optimization framework with second-order cone programming problems. Romeijn et al. [24] introduced a concept of C-VaR (conditional value-at-risk) that had been originally developed in financial engineering. Instead of DVCs, they used constraints that the *average* dose for a given fraction part should satisfy a given threshold. As pointed in [29], FMO problems with DVCs formulated in mathematical optimization problems often have multiple local minimum solutions and such problems are essentially NP-hard [26].

Among the above methods, an advantage of the C-VaR type constraints of Romeijn et al. [24] is that any irradiation intensity obtained from their LP problems satisfies all the DVCs. This property is not clearly mentioned in their paper, and we will verify it later in Lemma 2.2. They solved only one LP problem, therefore, its computation cost was not expensive. However, the feasible region of their LP problem was much narrow compared to the region intended by the DVCs. Since LP problems can be solved by a polynomial-time algorithms while the FMO problems themselves are NP-hard, we can not completely remove the gap between the C-VaR type constraints and the DVCs. In particular, the outliers seriously affected the average dose. This approach failed to find the beam intensities for some test instances of Task Group (TG) 119 report by the American

Association of Physicists in Medicine (AAPM) [11].

In this paper, we propose a successive LP approach that employs the C-VaR type constraints. We detect the outliers using LP problems which evaluate the deviation from the DVCs in the constraints, and remove the outliers successively from the domain of the C-VaR type constraints. We will show that if the objective value of the successive LP problems becomes non-positive, the proposed method outputs beam intensities that satisfy all the DVCs. The adjustment of the outliers by the successive LP problems enables the proposed method to search a wider region than the approach of Romeijn et al. In addition, the sequence of the objective values of the successive LP problems are non-increasing. This property implies that we can generate a sequence of the solutions that approaches to the DVCs. Since our optimization problems are still LP problems, the computation cost does not increase so much compared to the successive LP approach of Merrit et al. [16].

We conducted numerical tests to verify the performance of our approach. For test instances included in TG 119, our approach successfully found beam intensities that satisfied the DVCs within a few LP iterations. In addition, the solution of our approach satisfied the DVCs more appropriately than Merrit et al.

The rest of this paper is organized as follow. In Section 2, we first give a more precise definition and notation on DVCs and briefly discuss the formulations of Merrit et al. and Romeijn et al. In Section 3, we describe the details on our approach and, in Theorem 3.2, we give a proof of mathematical properties of our approach that are favorable for the FMO computation. Section 4 reports the numerical results on the TG 119 test instances. In Section 5, we will discuss several aspects of our approaches and extensions. Finally, we will give a conclusion in Section 6.

2 Preliminaries and Existing Formulation

As notation, we use $|S|$ to denote the cardinality of a set S . We take a nonnegative part of a number x by denoting $(x)^+ := \max\{x, 0\}$.

2.1 Preliminaries

To apply numerical computation to the IMRT problem in a practical way, the intended organs (or structures) and the radiation beams are often discretized into *voxels* (small cuboid units) and *beamlets*, respectively. Let S be the set of the structures. For each structure $s \in S$, we use V_s to denote the voxel set of s . Without loss of generality, we assume $|V_s| > 0$ throughout of this paper. In IMRT, the multi-leaf collimators make it possible to treat the radiation beam as a set of beamlet and control the intensity of each beamlet independently. The set of beamlet is denoted by B . The area radiated from each beamlet is usually $10 \text{ mm} \times 10 \text{ mm}$, $5 \text{ mm} \times 5 \text{ mm}$, $3 \text{ mm} \times 3 \text{ mm}$ and the number of beamlets $|B|$ is from hundreds to thousands. The order of the number of voxels is usually 10^4 .

It is often assumed that a dose of each voxel received from the beamlets is a linear function, therefore, the dose that the i th voxel in the s th structure receives can be expressed in $z_{si} = \sum_{j \in B} D_{sij} x_j$. Here, x_j is the intensity of the j th beamlet. The element D_{sij} is the (i, j) th element of a matrix $\mathbf{D}_s \in \mathbb{R}^{|V_s| \times |B|}$, and the matrix \mathbf{D}_s is called a fluence matrix and its element D_{sij} expresses the dose that the i th voxel in the s th structure receives from the unit intensity of the j th beamlet. To compute the fluence matrix, Naqvi et al. [19] utilized the Monte Carlo superposition. In the material below, we assume that the fluence matrix is given.

In a suitable treatment plan, its corresponding histogram should satisfy the DVCs. Precisely speaking, a DVC is identified by a structure s and a fractional parameter $\alpha \in (0, 1)$. We can

classify the DVCs into the two types, the upper and lower DVCs;

- (upper) The fraction of the voxels in the structure s that receive at least U_s^α Gy is at most α .
- (lower) The fraction of the voxels in the structure s that receive at least L_s^α Gy is at least α .

As an example, let us impose three DVCs to a tumor named PTV; $L_{\text{PTV}}^{0.9} = 50.0$, $L_{\text{PTV}}^{0.99} = 46.5$ and $U_{\text{PTV}}^{0.2} = 55.0$. In this case, at least 99% of the tumor PTV must receive at least 46.5 Gy. Furthermore, 90% of PTV should receive a higher dose than 50.0 Gy. At the same time, we should also avoid extremely strong intensity and this is expressed by the upper constraint of $U_{\text{PTV}}^{0.2}$, that is, 20% voxels or less of PTV can exceed 55.0 Gy. As shown in this example, the number of DVCs imposed for one tumor or organ can be larger than one.

In the following discussion, we will use \underline{A}_s and \overline{A}_s to denote the set of the fractions that are involved in the lower and upper DVCs of the structure s , respectively. For each $\alpha \in \overline{A}_s$, we associate the upper DVC whose threshold is U_s^α Gy. Similar notation is applied to $\alpha \in \underline{A}_s$ for the lower DVC with L_s^α Gy. In the DVC example above, we have $\underline{A}_{\text{PTV}} = \{0.9, 0.99\}$ and $\overline{A}_{\text{PTV}} = \{0.2\}$. In a mathematical form, a single upper DVC can be described as $\frac{|\{i \in V_s | z_{si} > U_s^\alpha\}|}{|V_s|} \leq \alpha$, and a single lower DVC as $\frac{|\{i \in V_s | z_{si} > L_s^\alpha\}|}{|V_s|} \geq \alpha$.

We assume that $\underline{A}_s \subset (0, 1)$ and $\overline{A}_s \subset (0, 1)$. For the specific fractional case corresponding to $\alpha = 0$ or $\alpha = 1$, we also denote the upper or lower bounds by U_s and L_s , respectively. When these threshold are used, *each* voxel in the structure s is required to receive the dose between L_s and U_s .

An FMO problem can now be casted as a mathematical problem to find the beamlet intensities that satisfy all the DVCs. If we are allowed to use mixed-integer programming problems, one goal in FMO is to find a solution of the feasible set \mathcal{F} defined by

$$\mathcal{F} := \{ \mathbf{x} \in \mathbb{R}^{|B|} : \begin{array}{ll} \sum_{j=1}^{|B|} D_{sij} x_j = z_{si} & \text{for } i = 1, \dots, |V_s|; s = 1, \dots, |S| \\ L_s \leq z_{si} \leq U_s & \text{for } i = 1, \dots, |V_s|; s = 1, \dots, |S| \\ z_{si} \geq 0 & \text{for } i = 1, \dots, |V_s|; s = 1, \dots, |S| \\ z_{si} \geq L_s^\alpha \underline{b}_{si}^\alpha & \text{for } i = 1, \dots, |V_s|; \alpha \in \underline{A}_s; s = 1, \dots, |S| \\ \underline{b}_{si}^\alpha \in \{0, 1\} & \text{for } i = 1, \dots, |V_s|; \alpha \in \underline{A}_s; s = 1, \dots, |S| \\ \sum_{i=1}^{|V_s|} \underline{b}_{si}^\alpha \geq \alpha |V_s| & \text{for } \alpha \in \underline{A}_s; s = 1, \dots, |S| \\ z_{si} \leq U_s^\alpha + M \overline{b}_{si}^\alpha & \text{for } i = 1, \dots, |V_s|; \alpha \in \overline{A}_s; s = 1, \dots, |S| \\ \overline{b}_{si}^\alpha \in \{0, 1\} & \text{for } i = 1, \dots, |V_s|; \alpha \in \overline{A}_s; s = 1, \dots, |S| \\ \sum_{i=1}^{|V_s|} \overline{b}_{si}^\alpha \leq \alpha |V_s| & \text{for } \alpha \in \overline{A}_s; s = 1, \dots, |S| \\ x_j \geq 0 & \text{for } j = 1, \dots, |B| \end{array} \}. \quad (1)$$

In this definition, a scalar M is so-called big-M, a constant number large enough. To express the fraction of the partial volume, the binary variables $\underline{b}_{si}^\alpha$ and \overline{b}_{si}^α are introduced. We should remark that a single upper DVC $|\{i \in V_s | z_{si} > U_s^\alpha\}| \leq \alpha |V_s|$ is imposed by a combination of $z_{si} \leq U_s^\alpha + M \overline{b}_{si}^\alpha$, $\overline{b}_{si}^\alpha \in \{0, 1\}$ and $\sum_{i=1}^{|V_s|} \overline{b}_{si}^\alpha \leq \alpha |V_s|$. The number of voxels exceeds thousands in practical situations, so the number of these binary variables are also considerably large. The set \mathcal{F} embraces properties of combinatorial sets and it is not an easy task to find a feasible point of \mathcal{F} exactly. As pointed in [26], such a task is NP-hard.

2.2 A successive linear programming method

In 2002, Merritt et al. [16] employed LP problems to formulate the FMO problem in a mathematical way and exploited the information obtained from the dual LP problems. Their method is refereed

as Method-M in the material below. A main idea of Method-M is to solve LPs successively searching better beamlet intensities. We now briefly introduce Method-M by a simple situation which involves one tumor structure ($s = 1$) and one healthy structure ($s = 2$). We consider hard DVC thresholds U_1 and U_2 on the tumor and the healthy structures, respectively, and use a soft DVC threshold U_2^α such that $U_2^\alpha \leq U_2$. A framework of Method-M for this situation is given as follow, and this framework can be easily extended to general cases of more DVCs.

Algorithm 2.1. [16] (*Method-M*) *A successive LP method for the FMO optimization*

1. Set the iteration number $k = 0$, and set an initial set $R_0 = \emptyset$. Set a parameter $\lambda > 0$ and a stopping threshold $\hat{\tau} > 0$.
2. Solve the following k th LP to determine the intensity of beamlets $\mathbf{x} \in \mathbb{R}^{|B|}$ and let τ_k be the optimal value of this LP.

$$\begin{array}{ll}
\text{maximize} & \tau \\
\text{subject to} & \sum_{j=1}^{|B|} D_{sij} x_j = z_{si} \quad \text{for } i = 1, \dots, |V_s|; s = 1, 2 \\
& \tau \leq z_{1i} \leq U_1 \quad \text{for } i = 1, \dots, |V_1| \\
& z_{2i} \leq U_2 \quad i \in R_k \\
& z_{2i} \leq U_2^\alpha \quad i \notin R_k \\
& z_{si} \geq 0 \quad \text{for } i = 1, \dots, |V_s|; s = 1, 2 \\
& x_j \geq 0 \quad \text{for } j = 1, \dots, |B|.
\end{array}$$

3. If $\tau_k > \hat{\tau}$, output the optimal solution of the k th LP and stop.
4. Update R_k with the rule $R_{k+1} = R_k \cup \{i \in V_2 \mid y_i^* > \lambda\}$, where y_i^* is the dual variable corresponding to the constraint $z_{2i} \leq U_2^\alpha$ in the k th LP.
5. Increment k and return to Step 2.

In the k th LP, each voxel in the tumor structure ($s = 1$) receives the dose at least τ , therefore, the aim in the k th LP is to maximize τ so that the voxels in the tumor receives as high dose as possible.

The usage of the hot-spot set R_k characterizes Method-M. Though it is preferable that each voxel in the healthy structure ($i \in V_2$) should be imposed by a low limit $z_{2i} \leq U_2^\alpha$, such a constraint is too restrictive to satisfy. Therefore, Merritt et al. relaxed this constraint so that a small set $R_k \subset V_2$ can be exposed to higher dose than U_2 (Note that $U_2 \geq U_2^\alpha$). These voxels, regarded as outliers, are determined using the information from the dual LP problem in Step 4. The updated hot-spot set R_{k+1} is composed of the voxels for which the lower limit $z_{2i} \leq U_2^\alpha$ is too restrictive.

In contrast, a disadvantage of this method is that it does not take the fractional parameter α of tumor into consideration. The constraints in the LP problem involve all the voxels in the structures, and they are much stronger than the DVCs. Since the feasible region has a tendency to become very narrow, this method may fail to find favorable beamlet intensities for DVCs.

2.3 An Approach Based on C-VaR type Constraints

Romeijn et al. [24, 23] also utilized LP problems to determine the beamlet intensities, but their approach brought a different perspective. Their method is refereed as Method-R in this paper. The

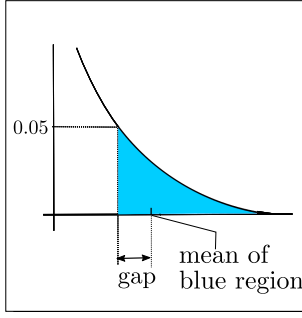


Figure 3: A comparison between DVC and C-VaR type constraint

key step of Method-R is to replace the DVCs with C-VaR type constraints in the LP problem, and only one LP problem is solved. C-VaR stands for *conditional value at risk*, and it was originally introduced by Rockafellar [22] in a context of economics. In economics, there is a demand for estimating the expected value of the loss that exceeds a certain level called Value at Risk (VaR). In particular, C-VaR has high affinity with a fraction.

For a random variable X and level α , the original definition of C-VaR computes an average of VaR using an integral as follow:

$$\text{CVaR}_{1-\alpha}(X) := \frac{1}{\alpha} \int_0^\alpha \text{VaR}_{1-\tau}(X) d\tau.$$

Here, we do not discuss a precise definition of VaR, since an equivalent but more convenient form of C-VaR is available:

$$\text{CVaR}_\alpha(X) := \min_{C \in \mathbb{R}} \left\{ C + \frac{1}{1-\alpha} E[(X - C)^+] \right\}. \quad (2)$$

A key step of Method-R is to replace a single upper DVC $|\{i \in V_s | z_{si} > U_s^\alpha\}| \leq \alpha |V_s|$ with a C-VaR type inequality

$$\min_{C \in \mathbb{R}} \left\{ C + \frac{1}{\alpha |V_s|} \sum_{i=1}^{|V_s|} (z_{si} - C)^+ \right\} \leq U_s^\alpha.$$

This inequality is equivalent to find $\bar{\zeta}_s^\alpha \in \mathbb{R}$ which satisfies

$$\bar{\zeta}_s^\alpha + \frac{1}{\alpha |V_s|} \sum_{i=1}^{|V_s|} (z_{si} - \bar{\zeta}_s^\alpha)^+ \leq U_s^\alpha. \quad (3)$$

The upper DVC imposes that the number of voxels that receive U_s^α or more is bounded by $\alpha |V_s|$. In contrast, the upper C-VaR type constraint (3) requires that the mean dose of the $\alpha |V_s|$ highest voxels be under U_s^α . Here, we use Figure 3 to compare DVC and the C-VaR type constraint in the DVH style. The upper DVC on $U_s^\alpha = 0.05$ requires the leftmost point of blue region be less than U_s^α . In contrast, the upper C-VaR corresponding to this DVC requires that the mean of blue region be less than U_s^α . Therefore, when U_s^α lies between the leftmost point and the mean, there is a difference between the DVC and the C-VaR type constraint. In Chapter 3, we will observe this in detail.

We can develop the inequality (3) in another way. For simplicity, we assume that $\alpha |V_s|$ is an integer number. Let us use $\mathcal{S}_k(\mathbf{z})$ for an integer k and $\mathbf{z} \in \mathbb{R}^n$ to denote the sum of the k largest

elements of \mathbf{z} . In [4, Example 9.10], it is shown that $\mathcal{S}_k(\mathbf{z}) \leq t$ is equivalent to a condition that there exists $\bar{\zeta}, t_1, t_2, \dots, t_n \in \mathbb{R}$ such that

$$\begin{cases} t \geq k\bar{\zeta} + (t_1 + t_2 + \dots + t_n) \\ t_1, t_2, \dots, t_n \geq 0 \\ t_1 - z_1 + \bar{\zeta} \geq 0, t_2 - z_2 + \bar{\zeta} \geq 0, t_n - z_n + \bar{\zeta} \geq 0. \end{cases} \quad (4)$$

Since the mean dose of the $\alpha|V_s|$ highest voxels should be less than U_s^α , we have $\frac{\mathcal{S}_{\alpha|V_s|}(\mathbf{z}_s)}{\alpha|V_s|} \leq U_s^\alpha$. Here, \mathbf{z}_s is the vector that collects the doses in the structure s , $\mathbf{z}_s := (z_{s1}, \dots, z_{s|V_s|})^T \in \mathbb{R}^{|V_s|}$. Applying (4) with $k = \alpha|V_s|$ and $t = \alpha|V_s| \cdot U_s^\alpha$, we can show that $\frac{\mathcal{S}_{\alpha|V_s|}(\mathbf{z}_s)}{\alpha|V_s|} \leq U_s^\alpha$ if and only if there exists $\bar{\zeta}_s^\alpha \in \mathbb{R}$ that satisfies (3).

By introducing the concept of C-VaR to the IMRT optimization, Romeijn et al. [24] proposed the following LP problem:

$$\text{minimize} \quad \sum_{s=1}^{|S|} \sum_{i=1}^{|V_s|} F_s(z_{si}) \quad (5a)$$

$$\text{subject to} \quad \sum_{j=1}^{|B|} D_{sij} x_j = z_{si} \quad i = 1, \dots, |V_s|; s = 1, \dots, |S| \quad (5b)$$

$$L_s \leq z_{si} \leq U_s \quad i = 1, \dots, |V_s|; s = 1, \dots, |S| \quad (5c)$$

$$\underline{\zeta}_s^\alpha - \frac{1}{(1-\alpha)|V_s|} \sum_{i=1}^{|V_s|} (\underline{\zeta}_s^\alpha - z_{si})^+ \geq L_s^\alpha \quad \alpha \in \underline{A}_s; s = 1, \dots, |S| \quad (5d)$$

$$\bar{\zeta}_s^\alpha + \frac{1}{\alpha|V_s|} \sum_{i=1}^{v_s} (z_{si} - \bar{\zeta}_s^\alpha)^+ \leq U_s^\alpha \quad \alpha \in \bar{A}_s; s = 1, \dots, |S| \quad (5e)$$

$$x_j \geq 0 \quad j = 1, \dots, |B| \quad (5f)$$

$$z_{si} \geq 0 \quad i = 1, \dots, |V_s|; s = 1, \dots, |S| \quad (5g)$$

$$\underline{\zeta}_s^\alpha, \bar{\zeta}_s^\alpha : \text{free variable} \quad (5h)$$

Here, the decision variables are the beamlet intensities $x_1, \dots, x_{|B|}$. To implement the C-VaR type constraints, intermediate variables $\underline{\zeta}_s^\alpha$ and $\bar{\zeta}_s^\alpha$ are employed.

They used piecewise a linear function F_s for the objective function in order to express an deviation from their desired situation, and this objective function remained (5) as an LP problem. Aleman et al. [1] examined quadratic penalty functions for the objective function to incorporate the deviation, and they applied interior-point methods to solve the resultant quadratic optimization problem.

The validity of C-VaR type constraints in (5) can be guaranteed by the following lemma. Though this claim was partially implied in [23], we give it in an explicit way.

Lemma 2.2. *Any feasible solution of (5) fulfills all the DVCs.*

Proof: From the constraint (5c), it is clear that the hard DVCs ($L_s \leq z_{si} \leq U_s$) are satisfied.

We now assume that a single upper DVC $|\{i \in V_s | z_{si} > U_s^\alpha\}| \leq \alpha|V_s|$ is violated, and we will derive a contradiction. From this assumption, the number of voxels such that $z_{si} > U_s^\alpha$ is greater than $\alpha|V_s|$. Since $U_s^\alpha \geq \bar{\zeta}_s^\alpha$ from (5e), it holds that $z_{si} > \bar{\zeta}_s^\alpha$ when $z_{si} > U_s^\alpha$. There exists at least one i such that $z_{si} > \bar{\zeta}_s^\alpha$, since $|\{i \in V_s | z_{si} > U_s^\alpha\}| > \alpha|V_s| \geq 0$ from our assumption, hence, we

have $(z_{si} - \bar{\zeta}_s^\alpha)^+ = z_{si} - \bar{\zeta}_s^\alpha > U_s^\alpha - \bar{\zeta}_s^\alpha$ for such i . It leads to

$$\bar{\zeta}_s^\alpha + \frac{1}{\alpha|V_s|} \sum_{i=1}^{|V_s|} (z_{si} - \bar{\zeta}_s^\alpha)^+ > \bar{\zeta}_s^\alpha + \frac{1}{\alpha|V_s|} (\alpha|V_s|) (U_s^\alpha - \bar{\zeta}_s^\alpha) = U_s^\alpha$$

and this contradicts to (5e). Hence, any feasible solution of (5) does not violate the upper DVC. A similar discussion can be applied to the lower DVCs (5d). \square

This lemma indicates an advantage of the LP model (5) that if a feasible solution is found in (5), it should fulfill all the DVCs. A negative side is that this approach may fail to find solutions that exist in the gap between the DVCs and the C-VaR type constraints (The converse of Lemma 2.2 does not hold in general). This approach searches only narrower feasible region than the original DVCs, and this aspect motivated us to develop a successive method that extends the feasible region from the C-VaR type constraints.

3 Successive Linear Programming Approach with C-VaR type Constraints

A main difficulty in handling the DVCs is that the DVCs involve the fraction α , hence finding a feasible solution is already a demanding task. Method-M utilized the hot-spot to remove some outliers from the strict constraints, and Method-R introduced the C-VaR type constraints to replace the original DVCs. A common problem arising from the two methods was that their search regions were not wide enough to cover the region shaped by the DVCs. Hence, the two methods sometimes fail to find a feasible solution, even when the original feasible set has enough space.

In particular, we observed from preliminary numerical tests that the C-VaR type constraints are sensitive to outliers in the sense that the voxels that have extremely high or low doses affect the constraints of (5) seriously.

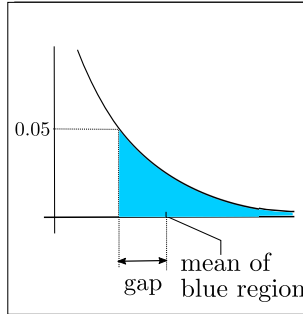


Figure 4: A DVH in which a few voxels receive extremely high doses

To illuminate such a phenomenon, we compare Figures 3 and 4 that partially illustrate different solutions of an FMO problem in the style of DVH. The two DVHs are almost same, but Figure 4 has a few voxels that receive extremely high doses. Their means of the blue region are quite different, and it indicates that the satisfiability of (5e) strongly depends on the voxels that have the highest doses. Such voxels should be handled carefully as outliers.

We propose a method that combines the successive update of outliers and the concept of the C-VaR type constraints. In the proposed method, we first solve an LP problem by relaxing the C-VaR constraints so that this LP problem always has a feasible point. From the optimal solution of this LP problem, we extract the outliers and transfer them from the domain of the C-VaR type

constraints (5e) to the sets of outliers. Using the new sets, we build a next LP problem. We repeat the updates of outliers until we obtain a feasible solution that satisfies the original DVCs. This new method has several favorable properties, and we will discuss them in Theorem 3.2.

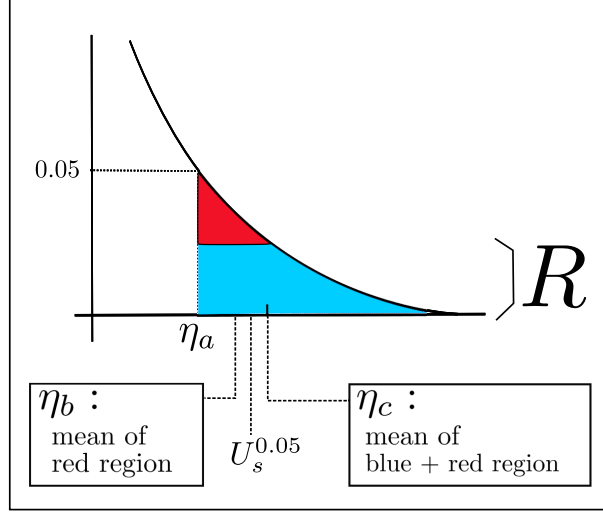


Figure 5: Effect of the exclusion of R

The comparison between an original DVC, its corresponding C-VaR type constraints and the constraint in the proposed method is summarized as an illustrative example of Figure 5. We denote the left endpoint of the blue and red areas by η_a . We also use η_b and η_c to denote the mean dose of the red area and that of blue and red areas, respectively. The value on this DVH at η_a is 0.05, therefore this solution satisfies an DVC of $U_s^{0.05}$ if and only if $\eta_a \leq U_s^{0.05}$. Similarly, $\eta_c \leq U_s^{0.05}$ if and only if the solution satisfies the C-VaR type constraint for U_s^α . From the discussion in the previous paragraphs, if $U_s^{0.05}$ in the interval $\eta_a < U_s^{0.05} < \eta_c$, this solution is a feasible solution of the FMO problem, even though the approach based on the C-VaR type constraints fails to recognize this solution as a feasible solution.

We consider an effect of excluding voxels that have highest doses by defining them as a set of outliers R . We evaluate the left-hand side of the C-VaR type constraint using only the rest of the voxels. In Figure 5, this corresponds to the removal of the blue regions, therefore, the left-hand side of the C-VaR type constraint is shifted from η_c to η_b . If $U_s^{0.05}$ is in the interval $\eta_b < U_s^{0.05} < \eta_c$, this new approach can detect this solution is feasible. This is the key idea of our approach.

The framework of the proposed method is summarized in Algorithm 3.1. In the k th LP problem of Step 2, we use $\overline{R}_s^{k,\alpha}$ and $\underline{R}_s^{k,\alpha}$ to denote the sets of outliers with respect to the thresholds $\alpha \in \overline{A}_s$ and $\alpha \in \underline{A}_s$, respectively. In addition, the objective function t is introduced to measure the deviation from the DVCs. The positive constants \overline{P}_s , \underline{P}_s , \overline{P}_s^α and \underline{P}_s^α are embedded to control the relaxation of the DVCs.

Algorithm 3.1. *A successive updates of outliers with C-VaR type constraints for FMO problems*

1. Set the iteration counter $k = 1$ and the initial sets of outliers $\overline{R}_s^{1,\alpha} = \emptyset$ for $\alpha \in \overline{A}_s, s \in S$ and $\underline{R}_s^{1,\alpha} = \emptyset$ for $\alpha \in \underline{A}_s, s \in S$. Choose positive constants \overline{P}_s and \underline{P}_s for $s \in S$, \overline{P}_s^α for $\alpha \in \overline{A}_s, s \in S$, and \underline{P}_s^α for $\alpha \in \underline{A}_s, s \in S$.
2. Solve the following k th LP. Let $t^{(k)}$ be the optimal value of this LP problem, and $x_j^{(k)}$ and

$z_{si}^{(k)}$ the obtained solution.

$$\min \quad t \quad (6a)$$

$$\text{s.t.} \quad \sum_{j=1}^{|B|} D_{sij} x_j = z_{si} \quad i \in V_s; s \in S \quad (6b)$$

$$z_{si} \leq U_s + \overline{P}_s t \quad i \in V_s; s \in S \quad (6c)$$

$$z_{si} \geq L_s - \underline{P}_s t \quad i \in V_s; s \in S \quad (6d)$$

$$\underline{\zeta}_s^\alpha - \frac{1}{(1-\alpha)|V_s| - |\underline{R}_s^{k,\alpha}|} \sum_{\substack{i=1 \\ i \notin \underline{R}_s^{k,\alpha}}}^{|V_s|} (\underline{\zeta}_s^\alpha - z_{si})^+ \geq L_s^\alpha - \underline{P}_s^\alpha t \quad \alpha \in \underline{A}_s; s \in S \quad (6e)$$

$$\overline{\zeta}_s^\alpha + \frac{1}{\alpha|V_s| - |\overline{R}_s^{k,\alpha}|} \sum_{i=1, i \notin \overline{R}_s^{k,\alpha}}^{|V_s|} (z_{si} - \overline{\zeta}_s^\alpha)^+ \leq U_s^\alpha + \overline{P}_s^\alpha t \quad \alpha \in \overline{A}_s; s \in S \quad (6f)$$

$$x_j \geq 0 \quad j \in B \quad (6g)$$

$$z_{si} \geq 0 \quad i \in V_s; s \in S \quad (6h)$$

$$\overline{\zeta}_s^\alpha : \text{free variable} \quad \alpha \in \overline{A}_s; s \in S \quad (6i)$$

$$\underline{\zeta}_s^\alpha : \text{free variable} \quad \alpha \in \underline{A}_s; s \in S \quad (6j)$$

$$t : \text{free variable}$$

3. If $t^{(k)} \leq 0$, output $\mathbf{x}^{(k)}$ as the solution and stop.

4. Update the sets of outliers by the rules

$$\overline{R}_s^{k+1,\alpha} := \left\{ i \in V_s : z_{si}^{(k)} > U_s^\alpha + \overline{P}_s^\alpha t^{(k)} \right\}, \quad \underline{R}_s^{k+1,\alpha} := \left\{ i \in V_s : z_{si}^{(k)} < L_s^\alpha - \underline{P}_s^\alpha t^{(k)} \right\}.$$

Increment k and return to Step 2.

The proposed method has the following suitable properties.

Theorem 3.2. *We assume that the feasible region \mathcal{F} of the FMO problem (1) is not empty. Then, for the LP problems solved in Algorithm 3.1, it holds that*

(a) *For any $k \geq 1$, the k th LP problem (6) has an optimal solution.*

(b) *If $t^{(k)} \leq 0$, the output solution $\mathbf{x}^{(k)}$ satisfies all the DVCs (that is, $\mathbf{x}^{(k)} \in \mathcal{F}$).*

(c) *The sequence $\{t^{(k)}\}$ is monotone non-increasing.*

Part (a) indicates that the solution $\mathbf{x}^{(k)}$ is well-defined through the execution of Algorithm 3.1. Part (b) gives a validity for the stopping criterion $t^{(k)} \leq 0$ in Step 3. Finally, we can infer from Part (c) that the sequence $\{\mathbf{x}^{(k)}\}$ has a tendency to approach to the set that satisfy all the DVCs.

We remark that the solution obtained from Method-R corresponds to $x^{(1)}$ of Algorithm 3.1 with the parameters $\overline{P}_s = \underline{P}_s = \overline{P}_s^\alpha = \underline{P}_s^\alpha = 0$ for all s and α . From Part(c), therefore, the proposed method is more flexible than Method-R.

Proof: For Part(a), we first consider the case $k = 1$ and discuss $k \geq 2$ by induction. At the beginning of $k = 1$, $\underline{R}_s^{1,\alpha}$ and $\overline{R}_s^{1,\alpha}$ are empty sets. The denominators, therefore, in (6e) and (6f) are not zero, as $|V_s| > 0$ without loss of generality and $0 < \alpha < 1$. The initial LP problem ($k = 1$)

is well-defined, and we can give a feasible solution explicitly by $x_j = 0$ ($j = 1, \dots, |B|$), $z_{si} = 0$ ($i = 1, \dots, |V_s|$, $s = 1, \dots, |S|$), $\bar{\zeta}_s^\alpha = 0$ ($\alpha \in \bar{A}_s$, $s = 1, \dots, |S|$), $\underline{\zeta}_s^\alpha = 0$ ($\alpha \in \underline{A}_s$, $s = 1, \dots, |S|$) and $t = \min_{s=1, \dots, |S|} \{L_s/\underline{P}_s, \min_{\alpha \in \underline{A}_s} \{L_s^\alpha/\underline{P}_s^\alpha\}\}$. Therefore, we know that

$$\begin{aligned} \bar{\zeta}_s^\alpha + \frac{1}{\alpha|V_s| - |\bar{R}_s^{k,\alpha}|} \sum_{i=1, i \notin \bar{R}_s^{k,\alpha}}^{|V_s|} (z_{si} - \bar{\zeta}_s^\alpha)^+ &= \bar{\zeta}_s^\alpha + \frac{1}{\alpha|V_s|} \sum_{i=1}^{|V_s|} (z_{si} - \bar{\zeta}_s^\alpha)^+ \\ &\geq \bar{\zeta}_s^\alpha + \frac{1}{|V_s|} \sum_{i=1}^{|V_s|} (z_{si} - \bar{\zeta}_s^\alpha)^+ = \frac{1}{|V_s|} \sum_{i=1}^{|V_s|} \left\{ \bar{\zeta}_s^\alpha + (z_{si} - \bar{\zeta}_s^\alpha)^+ \right\} \geq 0. \end{aligned}$$

The last inequality holds from an inequality $p + (q - p)^+ \geq 0$ for any $p \in \mathbb{R}$ and $q \geq 0$. From (6c) and (6f), the objective function t has a lower bound $t \geq \max \left\{ \max_{s=1, \dots, S} \{-U_s/\bar{P}_s\}, \max_{\alpha \in \bar{A}_s} \{-U_s^\alpha/\bar{P}_s^\alpha\} \right\}$. From the duality theorem of linear programming [6, etc], the initial LP problem has an optimal value $t^{(1)}$.

Next, we assume that the k th LP has its optimal value $t^{(k)}$ and optimal solution $x_i^{(k)}$ and $z_{si}^{(k)}$, and we examine the $(k+1)$ th LP. If the number of voxels in V_s such that $z_{si}^{(k)} > U_s^\alpha + \bar{P}_s^\alpha t^{(k)}$ and $i \notin \bar{R}_s^{k,\alpha}$ were no less than $\alpha|V_s| - \bar{R}_s^{k,\alpha}$, we would have

$$\begin{aligned} \bar{\zeta}_s^\alpha + \frac{1}{\alpha|V_s| - |\bar{R}_s^{k,\alpha}|} \sum_{i=1, i \notin \bar{R}_s^{k,\alpha}}^{|V_s|} (z_{si}^{(k)} - \bar{\zeta}_s^\alpha)^+ &> \bar{\zeta}_s^\alpha + \frac{1}{\alpha|V_s| - |\bar{R}_s^{k,\alpha}|} (\alpha|V_s| - |\bar{R}_s^{k,\alpha}|) (U_s^\alpha + \bar{P}_s^\alpha t^{(k)} - \bar{\zeta}_s^\alpha) \\ &= U_s^\alpha + \bar{P}_s^\alpha t^{(k)}, \end{aligned}$$

but this contradicts (6f). Hence, the number of voxels that will be newly added to $\bar{R}_s^{k+1,\alpha}$ is less than $\alpha|V_s| - \bar{R}_s^{k,\alpha}$, and this leads to

$$|\bar{R}_s^{k+1,\alpha}| < (\alpha|V_s| - \bar{R}_s^{k,\alpha}) + \bar{R}_s^{k,\alpha} = \alpha|V_s|. \quad (7)$$

For the lower DVCs, we also obtain $|\underline{R}_s^{k+1,\alpha}| < (1 - \alpha)|V_s|$. Therefore, the denominators in (6f) and (6e) are not zero again, and we can use the same discussion as the initial LP problem to derive that the $(k+1)$ th LP has an optimal value $t^{(k+1)}$. By induction, for any $k \geq 1$, the k th LP has its optimal value $t^{(k)}$.

For Part (b), from the definition of $\bar{R}_s^{k+1,\alpha} = \{i \in V_s : z_{si}^{(k)} > U_s^\alpha + \bar{P}_s^\alpha t^{(k)}\}$, the non-positivity of $t^{(k)}$ indicates that $\{i \in V_s : z_{si}^{(k)} > U_s^\alpha\} \subset \bar{R}_s^{k+1,\alpha}$. Using the upper bound of the size of $\bar{R}_s^{k+1,\alpha}$ obtained in (7), we have $|\{i \in V_s : z_{si}^{(k)} > U_s^\alpha\}| \leq |\bar{R}_s^{k+1,\alpha}| \leq \alpha|V_s|$ and this means the solution of k th LP problem satisfies the corresponding upper DVCs. We can also show that the solution with non-positive $t^{(k)}$ satisfies the lower DVCs in a similar way.

Finally, in order to verify the inequality $t^{(k+1)} \leq t^{(k)}$ of Part (c), we give a feasible solution of the $(k+1)$ th LP problem such that $t = t^{(k)}$. We set $t = t^{(k)}$, $x_j = x_j^{(k)}$, $z_{si} = z_{si}^{(k)}$, $\underline{\zeta}_s^\alpha = L_s^\alpha - \underline{P}_s^\alpha t^{(k)}$ and $\bar{\zeta}_s^\alpha = U_s^\alpha + \bar{P}_s^\alpha t^{(k)}$. Since these values are derived from the k th LP problem, it is easy to check that these values satisfy the constraints of (6) except (6f) and (6e). In (6f), the summation $\sum_{i=1, i \notin \bar{R}_s^{k+1,\alpha}}^{|V_s|} (z_{si} - \bar{\zeta}_s^\alpha)^+$ is zero due to $\bar{R}_s^{k+1,\alpha} = \{i \in V_s : z_{si}^{(k)} > U_s^\alpha + \bar{P}_s^\alpha t^{(k)}\}$ and $\bar{\zeta}_s^\alpha = U_s^\alpha + \bar{P}_s^\alpha t^{(k)}$. Therefore, the left-hand side of (6f) reduces to $U_s^\alpha + \bar{P}_s^\alpha t^{(k)}$ and this is same as the right-hand side. Again, we apply a similar step to (6e). \square

4 Numerical Experiment

We used a dataset of the American Association of Physicists in Medicine (AAPM) Task Group (TG) 119 report [11]. The dataset includes four mock test cases; a C-shape case, a mock prostate case, a mock head/neck case and a multi target case. Table 1 is a summary of the dataset. For these four cases, the table shows the number of beamlet, the organ names, the number of voxels in the organs and the DVCs.

We compare the proposed method with Method-M (the successive LP method of Merrit et al. [16]) to demonstrate the performance of the proposed method. We did not include Method-R (the C-VaR method of Romeijn et al. [24]) for the comparison, since we found from preliminary experiments that the LP problems in the Method-R for all of the four test cases in AAPM TG119 were infeasible.

The dataset of AAPM TG119 is provided as 3D image format called DICOM. Using the CERR software 4.0 Beta 2 [8] and MATLAB 2013b, we transformed the DICOM files into the LP problems (6). We ran CERR with its default settings. Then, we called CPLEX 12.6.0 to solve the generated LP problems. Finally, we again utilized CERR to visualize the solutions and checked whether the obtained solutions satisfied the DVCs. We also used CERR to prepare a manageable dataset from the TG119 dataset. The number of voxels in the PTV organ of the mock head/neck case was more than 50,000 and this was too large to solve (6) on 16 GB memory space of our computing environment. For only this case, therefore, we chose 10,000 voxels randomly from the 50,000 voxels. We examined a number of this random selection and we observed this operation did not affect the numerical results so much. The computing environment was Windows 8 run on an Intel Core i7-4790 (3.6 GHz, 4 cores) and 16 GB of memory space.

A desirable stopping criterion of the proposed method is $t^{(k)} \leq 0$, since Theorem 3.2 showed that the output solution $\mathbf{x}^{(k)}$ satisfies all the DVCs when $t^{(k)} \leq 0$. Due to the intrinsic difficulty arising from combinatorial aspects of the DVCs, the number of iterations to attain $t^{(k)} \leq 0$ would be prohibitive. As a practical stopping criterion, we stop the proposed method when the iteration count k reaches 5 and output $\mathbf{x}^{(5)}$.

For the numerical computation of Method-M (Algorithm 2.1), we should describe configurations more specifically. The description for Method-M in Section 2.2 discussed only one tumor structure and only one healthy structure. To compute multiple tumors for Multi Target case, we associated τ_s for each tumor structure, and we maximized $\sum \tau_s$ over all of the tumor structure. Next, we set the parameter $\lambda = 10^{-6}$. Finally, we stopped Method-M when the set R became infeasible on a DVC; more precisely, when $|R_s^\alpha|$ exceeded $\alpha|V_s|$. When the infeasibility was detected at the k th iteration, the solution of Method-M was extracted from the solution of $(k - 1)$ th iteration.

For the execution of the proposed method, we need to specify values for positive constants $\underline{P}_s, \overline{P}_s, \underline{P}_s^\alpha, \overline{P}_s^\alpha$. We assigned 1 to these constants for all the cases except the C-shape case. For the C-shape case, we will explain more details later.

4.1 Results

Table 2 reports whether the obtained solutions satisfies DVCs or not. In addition, we also provide the DVH figures in Figures 6, 7, 8, and 9. In these figures, the solid lines and the broken lines indicate the results of the proposed method and Method-M, respectively, and different colors are used to clarify the organs.

In Table 2, the column ‘‘Proposed’’ shows the evaluation results of the solution obtained by the proposed method in the viewpoint of DVCs. For example, the value 50.3 in the row $L_{\text{Outer Target}}^{0.95}$ indicates that 95% of Outer Target receives at least 50.3 Gy. Therefore, this solution satisfies $L_{\text{Outer Target}}^{0.95} = 50.0$ and this is indicated by ‘‘Pass.’’ The failure of the solutions are indicated by

Table 1: A summary of the dataset for numerical comparison

C-shape (The number of beamlets is 414)		
organ/tumor	The number of voxels	DVCs
Outer Target	17522	$L_{\text{Outer Target}}^{0.95} = 50$ $U_{\text{Outer Target}}^{0.1} = 55$
Core	3087	$U_{\text{Core}}^{0.1} = 25$
Mock Head/Neck (The number of beamlets is 619)		
organ/tumor	The number of voxels	DVCs
PTV	10000	$L_{\text{PTV}}^{0.99} = 46.5$ $L_{\text{PTV}}^{0.9} = 50.0$ $U_{\text{PTV}}^{0.2} = 55$
Cord	1333	$U_{\text{Cord}} = 40$
Lt Parotid	525	$U_{\text{Lt Parotid}}^{0.5} = 20$
Rt Parotid	740	$U_{\text{Rt Parotid}}^{0.5} = 20$
Mock Prostate (The number of beamlets is 241)		
organ/tumor	The number voxels	DVCs
ProstatePTV	8591	$L_{\text{ProstatePTV}}^{0.95} = 75.6$ $U_{\text{ProstatePTV}}^{0.05} = 83$
Bladder	5207	$U_{\text{Bladder}}^{0.30} = 70$ $U_{\text{Bladder}}^{0.10} = 75$
Rectum	1830	$U_{\text{Rectum}}^{0.30} = 70$ $U_{\text{Rectum}}^{0.10} = 75$
Multi Target (The number of beamlets is 601)		
organ/tumor	The number of voxels	DVCs
Center	5143	$L_{\text{Center}}^{0.99} = 50$ $U_{\text{Center}}^{0.1} = 53$
Superior	5549	$L_{\text{Superior}}^{0.99} = 25$ $U_{\text{Superior}}^{0.1} = 35$
Inferior	5529	$L_{\text{Inferior}}^{0.99} = 12.5$ $U_{\text{Inferior}}^{0.1} = 25$

“Failed” in the table. In the same way, the column “Method-M” shows the result of Method-M. The table also reports the numbers of LP problems solved in each test case. The number of the parenthesis in the “Proposed” column means that the number of LP problems for the proposed method to acquire a feasible solution. In C-shape, for example, the proposed method obtained a feasible solution by the third LP problem ($t^{(3)} \leq 0$), and improved the solution with the successive two LP problems. (In the Multi Target case, we used (–) to indicate that we failed to obtain a non-negative optimal value.)

From the result of Table 2, we observe for the C-Shape case that the solution of the proposed method satisfies all DVCs. Method-M failed in the DVC $L_{\text{Outer Target}}^{0.95} = 50.0$. We also see that the green dashed line passes the point (50, 0.5) in Figure 6. This indicates that in the solution of the Method-M, a half of the voxels in OuterTarget receives less than 50Gy. We can further acquire similar observations on the Head/Neck case and the Prostate case.

For the Multi Target case, however, Table 2 shows that the solution of the proposed method fails to satisfy all DVCs. This means that the solution is far from a favorable solution. In addition, the shapes of the proposed method in Figure 9 are gradual slopes. In contrast, Method-M has a narrow width and outputs a better solution than the proposed method for only the Multi Target case.

Since the proposed method outputs solutions that matches the DVCs more adequately than Method-M for three problems out of the four cases, the proposed method has a tendency to output favorable solutions than Method-M. Furthermore, Table 2 shows that the numbers of iterations in the proposed method were at most 5. This implies that the proposed is better than Method-M from the viewpoint of computation cost.

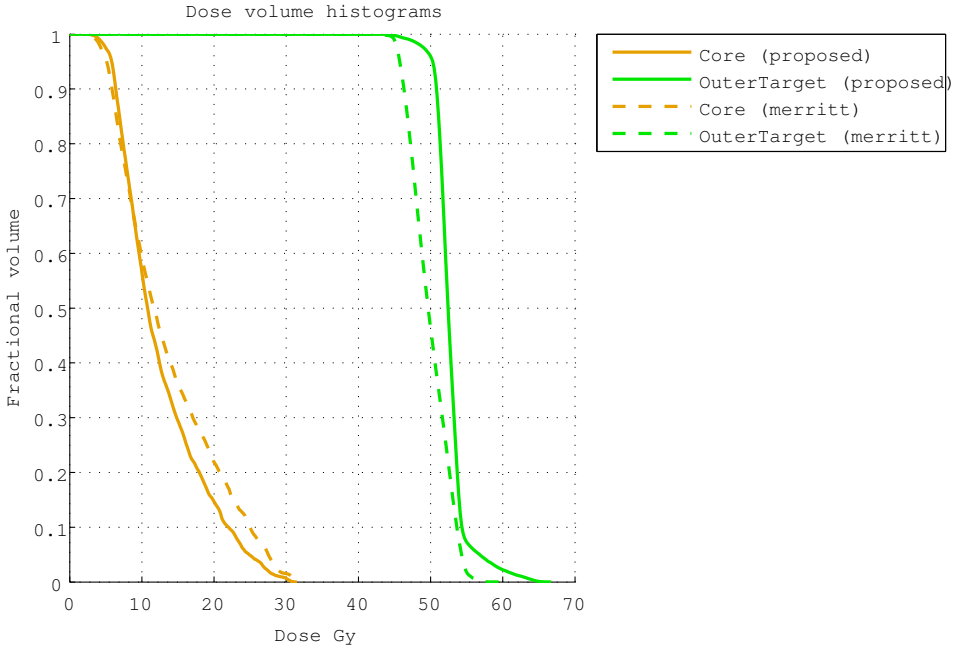


Figure 6: DVH of C-Shape case

Table 2: Numerical results for the four test cases

C-Shape			
organ/tumor	DVCs	Proposed	Method-M
Outer Target	$L_{\text{Outer Target}}^{0.95} = 50.0$	50.3 (Pass)	45.7 (Fail)
	$U_{\text{Outer Target}}^{0.10} = 55.0$	54.3 (Pass)	53.6 (Pass)
Core	$U_{\text{Core}}^{0.10} = 25.0$	22.0 (Pass)	25.0 (Pass)
the number of iterations		5(3)	14
Mock Head/Neck			
organ/tumor	DVCs	Proposed	Method-M
PTV	$L_{\text{PTV}}^{0.99} = 46.5$	47.6 (Pass)	38.4 (Fail)
	$L_{\text{PTV}}^{0.90} = 50.0$	51.2 (Pass)	40.5 (Fail)
	$U_{\text{PTV}}^{0.20} = 55.0$	53.5 (Pass)	51.2 (Pass)
Core	$U_{\text{Core}} = 40.0$	39.1 (Pass)	41.3 (Fail)
Lt Parotid	$U_{\text{Lt Parotid}}^{0.50} = 20.0$	17.5 (Pass)	20.4 (Fail)
Rt Parotid	$U_{\text{Rt Parotid}}^{0.50} = 20.0$	17.5 (Pass)	16.4 (Pass)
the number of iterations		5(3)	27
Prostate			
organ/tumor	DVCs	Proposed	Method-M
Prostate PTV	$L_{\text{Prostate PTV}}^{0.95} = 75.6$	78.1 (Pass)	74.7 (Fail)
	$U_{\text{Prostate PTV}}^{0.05} = 83.0$	82.3 (Pass)	82.2 (Pass)
Bladder	$U_{\text{Bladder}}^{0.30} = 70.0$	48.8 (Pass)	48.7 (Pass)
	$U_{\text{Bladder}}^{0.10} = 75.0$	72.5 (Pass)	64.5 (Pass)
Rectum	$U_{\text{Rectum}}^{0.30} = 70.0$	68.1 (Pass)	70.2 (Pass)
	$U_{\text{Rectum}}^{0.10} = 75.0$	74.3 (Pass)	74.8 (Pass)
the number of iterations		5(2)	22
Multi Target			
organ/tumor	DVCs	Proposed	Method-M
Center	$L_{\text{Center}}^{0.99} = 50.0$	48.2 (Fail)	43.5 (Fail)
	$U_{\text{Center}}^{0.10} = 53.0$	54.6 (Fail)	52.1 (Pass)
Inferior	$L_{\text{Inferior}}^{0.99} = 12.5$	10.8 (Fail)	21.7 (Pass)
	$U_{\text{Inferior}}^{0.10} = 25.0$	26.6 (Fail)	24.9 (Pass)
Superior	$L_{\text{Superior}}^{0.99} = 25.0$	23.3 (Fail)	33.3 (Pass)
	$U_{\text{Superior}}^{0.10} = 35.0$	36.5 (Fail)	34.9 (Pass)
the number of iterations		5(-)	15

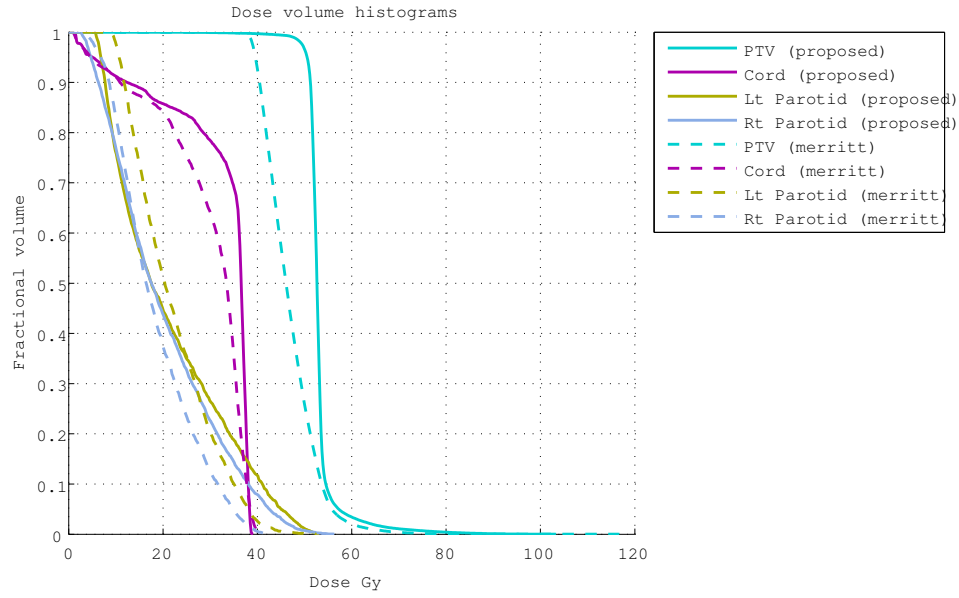


Figure 7: DVH of Head/Neck case

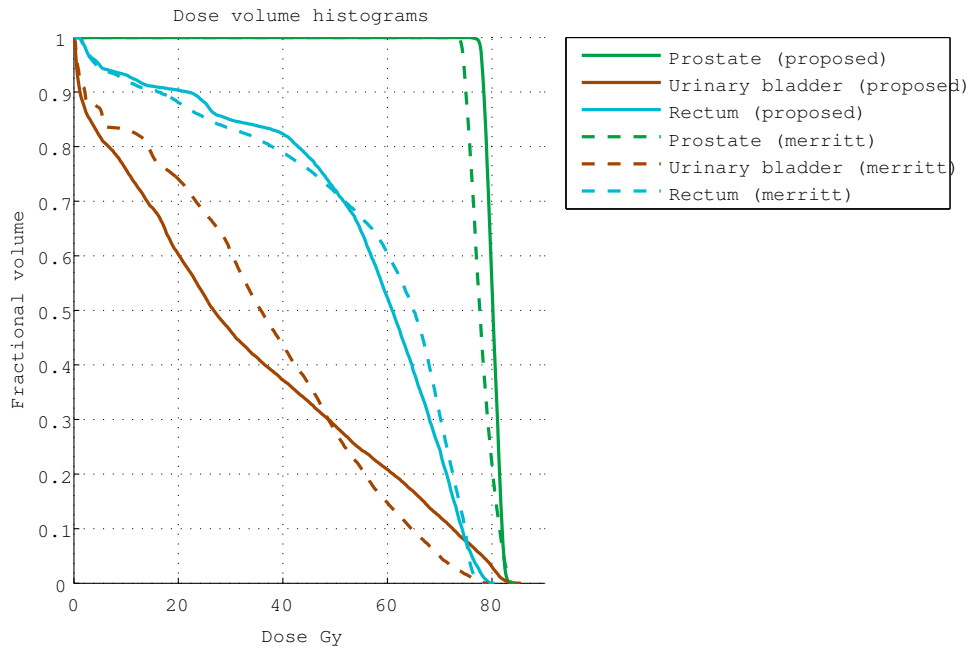


Figure 8: DVH of Prostate case

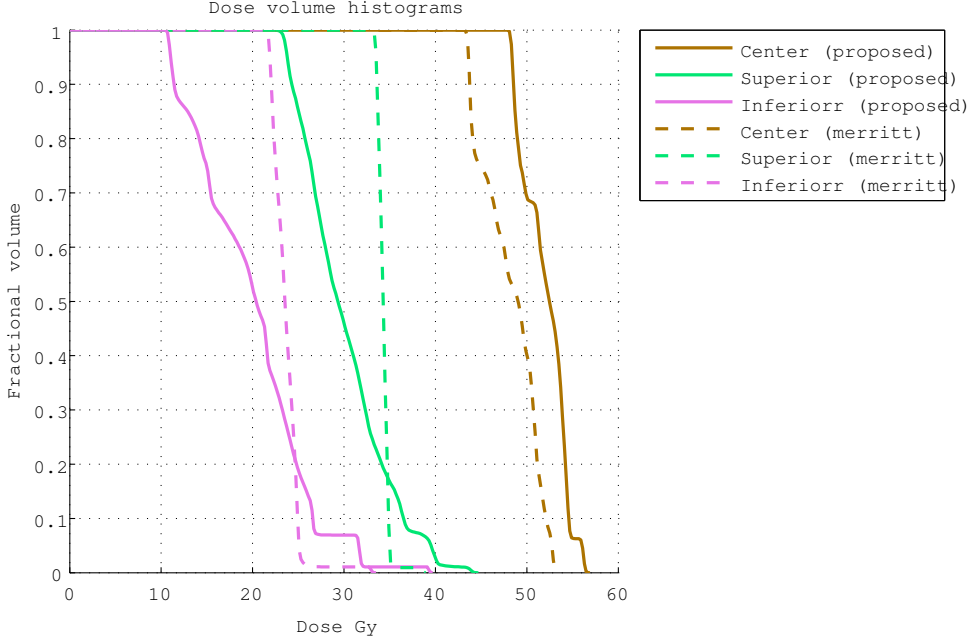


Figure 9: DVH of Multi target case

5 Discussions

In this paper we propose a new iterative algorithm for the FMO problems. Here, we discuss several aspects of the proposed method.

The result on Multi Target

The results on the Multi Target case imply a weakness of the proposed method. We have two reasons that the proposed method did not work properly for this test case. First, the concept of our method is to get a better solution by adjusting unsatisfied inequalities in the LP problem (6). Hence, the solution in a next iteration often improves the satisfiability of the unsatisfied inequalities. At the same time, however, this may bring a negative effect on the inequalities that are already satisfied. In particular, if there are hard constraints (with L_s and U_s) and soft constraints (with L_s^α and U_s^α) together in one problem, the soft constraints are influenced by the hard constraints and they sometime become infeasible even when there are feasible solutions that fulfill these soft constraints. Second, Ezzel et al. [11] pointed out that the Multi Target case is a difficult test case. They confirmed from statistics that for cases like the Multi Target case, even treatment planners often generate a solution that do not satisfy DVCs. For such cases, we should employ a different criterion instead of pursuing DVCs.

Parameters for Method-M

There would be a possibility that a careful selection on the parameters for Method-M might improve the quality of the solution or the running time. In the numerical experiments, we examined Method-M changing the parameters and we reported the best results of Method-M from the different parameters, so further improvements only by the parameter selection are not so promising.

For Method-M, a reduction of the computation time is also a daunting task. The test cases we used have a few DVC. To solve one LP problem, the proposed method consumed 2-3 times

computation time of Method-M. However, the proposed method acquired a feasible solution in two or three iterations. To compete the proposed method, therefore, Method-M should complete its algorithm with at most ten iterations, but Method-M required at least 14 iterations as shown in Table 2. We remark that the number of intermediate variables in the LP problems of the proposed method depends on the number of DVCs, while that of Method-M is independent from the number of DVCs. Therefore, Method-M may perform well in a test case with a large number of DVCs.

An extension of our approach for precise volumes

Another issue from a different viewpoint is the volume of each voxel. In this paper, we assumed that an organ was divided into voxels of the same rectangular shape, thus all the voxels had the same volume. However, voxels at the boundary of an actual structure may partially contain exterior of the structure. Therefore, there may be a difference between the total volume of voxels in the structure and the actual volume, and our approach would output a solution with serious deviations.

Our approach can be extended to handle the precise volume of each voxel by the steps below. For the i th voxel of the structure s , c_{si} is used to denote the volume of a part of s that is covered by the i th voxel, in other words, c_{si} is the volume of the intersection of s and the i th voxel. Then, a constant value $C_s := \sum_{i=1}^{v_s} c_{si}$ denotes the actual volume of s . We also define a new set for outliers $\bar{C}_s^{k,\alpha} := \sum_{i \in \bar{R}_s^{k,\alpha}} c_{si}$ for an upper DVC. In addition, $\underline{C}_s^{k,\alpha}$ is introduced for an lower DVC

We replace the k th LP problem in Algorithm 3.1 with the following LP problem:

$$\text{minimize } t \quad (8a)$$

$$\text{subject to } \sum_{j=1}^{N_b} D_{sij} x_j = z_{si} \quad i \in V_s; s \in S \quad (8b)$$

$$L_s - \underline{P}_s t \leq z_{si} \leq U_s + \bar{P}_s t \quad i \in V_s; s \in S \quad (8c)$$

$$\underline{\zeta}_s^\alpha - \frac{1}{(1-\alpha)C_s - \underline{C}_{ks}^\alpha} \sum_{i \notin \underline{R}_s^{k,\alpha}} c_{si} (\underline{\zeta}_s^\alpha - z_{si})^+ \geq L_s^\alpha - \underline{P}_s^\alpha t \quad \alpha \in \underline{A}_s; s \in S \quad (8d)$$

$$\bar{\zeta}_s^\alpha + \frac{1}{\alpha C_s - \bar{C}_s^{k,\alpha}} \sum_{i \notin \bar{R}_s^{k,\alpha}} c_{si} (z_{si} - \bar{\zeta}_s^\alpha)^+ \leq U_s^\alpha + \bar{P}_s^\alpha t \quad \alpha \in \bar{A}_s; s \in S \quad (8e)$$

$$x_j \geq 0 \quad j \in B \quad (8f)$$

$$z_{si} \geq 0 \quad i \in V_s; s \in S \quad (8g)$$

$$\underline{\zeta}_s^\alpha, \bar{\zeta}_s^\alpha, t : \text{free variables} \quad (8h)$$

A main difference between the original proposed method and this extended method lies in (6e) and (8d). In the original proposed method, we use the number of voxels to represent fractional volume of a structure. However, in the extended method, we use their actual volumes of voxels. Therefore, we include c_{si} in the summation of (8d). This LP problem satisfies the same property as Theorem 3.2. In particular, we can find a solution that satisfies all the DVCs when the optimal value $t^{(k)}$ of the k th LP problem is non-positive. Therefore, we can naturally extend the proposed method to handle the actual volumes.

6 Conclusion and Future Directions

In this paper, we proposed a new method for FMO problems using the C-VaR type constraints of Romeijn et al. and the outliers of Merrit et al. The proposed method has favorable mathematical

properties as discussed in Theorem 3.2. In particular, when the optimal value of the LP problems is non-positive, its optimal solution satisfies all the DVCs. From the numerical experiments, we verified that the proposed method was effective for the mock case. Particularly, the proposed method found feasible solutions for the test cases whose feasibilities were not detected by the LP problems of Romeijn et al. Furthermore, our approach obtained these feasible solutions within a shorter computation time than the approach of Merrit et al.

Further studies should include the removal of the two weaknesses in the proposed method. The first one is to get a better solution for the Multi-Target case and similar cases. Though these cases are very hard as discussed in Section 5, deep investigation the effect of the parameters involved in the LP problems could improve the situation. In particular, we need a discussion on adaptive selections of \underline{P}_s^α and \overline{P}_s^α . The other issue is a strong dependence of the size of LP problems on the number of DVCs. The size of the LP problems in the proposed method grows rapidly, when the number of DVCs increases. As a result, the size of solvable FMO problems are limited. We should reduce the number of variables involved in the LP problems by detecting redundant variables or inactive constraints.

References

- [1] D. M. Aleman, D. Glaser, H. E. Romeijn, and J. F. Dempsey. Interior point algorithms: guaranteed optimality for fluence map optimization in IMRT. *Physics in Medicine and Biology*, 55(18):5467, 2010.
- [2] G. Bednarz, D. Michalski, C. Houser, M. S. Huq, Y. Xiao, P. R. Anne, and J. M. Galvin. The use of mixed-integer programming for inverse treatment planning with pre-defined field segments. *Physics in Medicine and Biology*, 47(13):2235, 2002.
- [3] D. Bertsimas, V. Cacchiani, D. Craft, and O. Nohadani. A hybrid approach to beam angle optimization in intensity-modulated radiation therapy. *Computers & Operations Research*, 40(9):2187–2197, 2013.
- [4] G. C. Calafiore and L. El Ghaoui. *Optimization models*. Cambridge university press, 2014.
- [5] M. Chu, Y. Zinchenko, S. G. Henderson, and M. B. Sharpe. Robust optimization for intensity modulated radiation therapy treatment planning under uncertainty. *Physics in Medicine and Biology*, 50(23):5463, 2005.
- [6] V. Chvatal. *Linear programming*. Macmillan, 1983.
- [7] D. Craft. Local beam angle optimization with linear programming and gradient search. *Physics in Medicine and Biology*, 52(7):N127, 2007.
- [8] J. O. Deasy, A. I. Blanco, and V. H. Clark. Cerr: a computational environment for radiotherapy research. *Medical physics*, 30(5):979–985, 2003.
- [9] J. Dias, H. Rocha, B. Ferreira, and M. do Carmo Lopes. A genetic algorithm with neural network fitness function evaluation for IMRT beam angle optimization. *Central European Journal of Operations Research*, 22(3):431–455, 2014.
- [10] D. Djajaputra, Q. Wu, Y. Wu, and R. Mohan. Algorithm and performance of a clinical IMRT beam-angle optimization system. *Physics in Medicine and Biology*, 48(19):3191, 2003.

- [11] G. A. Ezzell, J. W. Burmeister, N. Dogan, T. J. LoSasso, J. G. Mechalakos, D. Mihailidis, A. Molineu, J. R. Palta, C. R. Ramsey, B. J. Salter, et al. IMRT commissioning: multiple institution planning and dosimetry comparisons, a report from AAPM task group 119. *Medical physics*, 36(11):5359–5373, 2009.
- [12] S. Gao, R. Meyer, W. D’Souza, L. Shi, and H. Zhang. A machine learning-based nested partitions framework for angle selection in radiotherapy. *Optimization Methods and Software*.
- [13] H. W. Hamacher and K. H. Küfer. Inverse radiation therapy planning — a multiple objective optimization approach. *Discrete Applied Mathematics*, 118(1):145–161, 2002.
- [14] National Cancer Institute. Radiation therapy for cancer. <http://www.cancer.gov/about-cancer/treatment/types/radiation-therapy/radiation-fact-sheet>. [Online; accessed 25-April-2016].
- [15] A. Matsuda, T. Matsuda, A. Shibata, K. Katanoda, T. Sobue, H. Nishimoto, and The Japan Cancer Surveillance Research Group. Cancer incidence and incidence rates in japan in 2008: A study of 25 population-based cancer registries for the monitoring of cancer incidence in japan (MCIJ) project. *Japanese Journal of Clinical Oncology*, 44(4):388–396, 2013.
- [16] M. Merritt, Y. Zhang, H. Liu, and R. Mohan. A successive linear programming approach to IMRT optimization problem. Technical Report 41, Dept. of Computational and Applied Mathematics Rice University Patents, 2002.
- [17] Labour Ministry of Health and Welfare. On countmeasures against cancers (in Japanese). <http://www.mhlw.go.jp/stf/shingi/2r9852000001sp25-att/2r9852000001spdf.pdf>. [Online; accessed 25-April-2016].
- [18] S. M. Morrill, R. G. Lane, J. A. Wong, and I. I. Rosen. Dose-volume considerations with linear programming optimization. *Medical Physics*, 18(6):1201–1210, 1991.
- [19] S. A. Naqvi, M. A. Earl, and D. M. Shepard. Convolution/superposition using the monte carlo method. *Physics in medicine and biology*, 48(14):2101, 2003.
- [20] A. Olafsson and S. J. Wright. Efficient schemes for robust imrt treatment planning. *Physics in medicine and biology*, 51(21):5621, 2006.
- [21] P. M. Pardalos and H. E. Romeijn. *Handbook of optimization in medicine*, volume 5. Springer Science & Business Media, 2009.
- [22] R. T. Rockafellar and S. Uryasev. Optimization of conditional value-at-risk. *Journal of risk*, 2:21–42, 2000.
- [23] H. E. Romeijn, R. K. Ahuja, J. F. Dempsey, and A. Kumar. A new linear programming approach to radiation therapy treatment planning problems. *Operations Research*, 54(2):201–216, 2006.
- [24] H. E. Romeijn, R. K. Ahuja, J. F. Dempsey, A. Kumar, and J. G. Li. A novel linear programming approach to fluence map optimization for intensity modulated radiation therapy treatment planning. *Physics in Medicine and Biology*, 48(21):3521, 2003.
- [25] D. M. Shepard, M. A. Earl, X. A. Li, S. Naqvi, and C. Yu. Direct aperture optimization: a turnkey solution for step-and-shoot IMRT. *Medical physics*, 29(6):1007–1018, 2002.

- [26] A. T. Tuncel, F. Preciado, R. L. Rardin, M. Langer, and J. P. P. Richard. Strong valid inequalities for fluence map optimization problem under dose-volume restrictions. *Annals of Operations Research*, 196(1):819–840, 2012.
- [27] B. van Asselen, M. Schwarz, C. van Vliet-Vroegindeweij, J. V. Lebesque, B. J. Mijnheer, and E. M. F. Damen. Intensity-modulated radiotherapy of breast cancer using direct aperture optimization. *Radiotherapy and oncology*, 79(2):162–169, 2006.
- [28] X. Wang, X. Zhang, L. Dong, H. Liu, Q. Wu, and R. Mohan. Development of methods for beam angle optimization for IMRT using an accelerated exhaustive search strategy. *International Journal of Radiation Oncology* Biology* Physics*, 60(4):1325–1337, 2004.
- [29] Q. Wu and R. Mohan. Multiple local minima in IMRT optimization based on dose-volume criteria. *Medical physics*, 29(7):1514–1527, 2002.
- [30] H. H. Zhang, R. R. Meyer, J. Wu, S. A. Naqvi, L. Shi, and W. D’Souza. A two-stage sequential linear programming approach to IMRT dose optimization. *Physics in medicine and biology*, 55(3):883, 2010.